

## Quantum Parametric Oscillator with Trapped Ions

Shiqian Ding,<sup>1</sup> Gleb Maslennikov,<sup>1</sup> Roland Hablützel,<sup>1</sup> Huanqian Loh,<sup>1</sup> and Dzmitry Matsukevich<sup>1,2</sup>

<sup>1</sup>Centre for Quantum Technologies, National University of Singapore, 3 Science Drive 2, 117543 Singapore, Singapore

<sup>2</sup>Department of Physics, National University of Singapore, 2 Science Drive 3, 117551 Singapore, Singapore

(Received 20 May 2016; published 12 October 2017)

A strong nonlinear coupling between harmonic oscillators is highly desirable for quantum information processing and quantum simulation, but is difficult to achieve in many physical systems. Here, we exploit the Coulomb interaction between two trapped ions to achieve strong nonlinear coupling between normal modes of motion at the single-phonon level. We experimentally demonstrate phonon up- and down-conversion and apply this coupling to directly measure the parity and Wigner functions of the ions' motional states. Our results represent the fully quantum operation of a degenerate parametric oscillator and hold promise for quantum computation schemes that involve continuous variables.

DOI: 10.1103/PhysRevLett.119.150404

A system of harmonic oscillators coupled via nonlinear interaction, first studied in mechanical systems in the nineteenth century [1], is a fundamental model in many branches of physics, from biophysics to electronics and condensed matter. In quantum optics, weak nonlinear interaction between light modes has enabled the generation of squeezed states and entangled photons [2]. However, stronger interactions are required for numerous applications of quantum computation and simulation [3–9]. While strong nonlinear interaction between modes has been demonstrated in circuit QED [10,11], achieving significant coupling with single quanta in other physical systems remains a challenge [3,12].

Cold atomic ions confined in rf Paul traps provide a well-established system for quantum information processing because it allows for perfect control and long coherence times of both internal and motional states [13]. Trapped ions experience a pseudopotential that is harmonic to a high degree and their motion is usually approximated by a set of noninteracting normal modes. Coulomb interaction between the ions is, however, nonlinear and can introduce coupling between the modes and anharmonicity to the ion motion [14,15]. The linear coupling of motional modes due to mutual Coulomb repulsion of ions in independent potential wells was previously demonstrated in the quantum regime [16,17]. The higher order terms in the Coulomb interaction lead, for example, to a cross-Kerr-type nonlinear coupling that shifts the normal mode frequencies [14,15] which has been experimentally observed [18]. The nonlinear interactions between internal and motional states of a single trapped ion have also been reported [19].

Here, we use two cotrapped ions to demonstrate a strong nonlinear interaction between two normal modes of motion that is equivalent to a degenerate parametric oscillator [2]. We consider a system of two ions with the same mass  $m$  and charge  $e$  in a linear Paul trap with single-ion secular

frequencies  $\omega_x, \omega_y, \omega_z$ . The potential energy of the system is [14,15]

$$V = m\omega_x^2(X^2 + x^2) + m\omega_y^2(Y^2 + y^2) + m\omega_z^2(Z^2 + z^2) + \frac{e^2}{8\pi\epsilon_0} \frac{1}{\sqrt{x^2 + y^2 + z^2}}, \quad (1)$$

where  $\epsilon_0$  is the permittivity of free space,  $X, Y, Z$  are the center-of-mass coordinates, and  $x, y, z$  are half the separation between the ions along the direction of principle trap axes. When  $\omega_z < (\omega_x, \omega_y)$ , the ions crystallize along the axial ( $z$ ) direction at an equilibrium distance  $z_0$  from the trap center. According to Eq. (1), the motion of the center-of-mass modes is harmonic, but the out-of-phase modes are coupled by the Coulomb interaction. For small axial displacement  $u = z - z_0$  and keeping only terms up to the third order that contribute to the coupling between the  $x$  and  $z$  modes, the potential energy becomes [15]

$$V = m\omega_r^2 x^2 + m\omega_s^2 u^2 + \frac{m\omega_s^2}{z_0} x^2 u + \dots$$

Here,  $\omega_s = \sqrt{3}\omega_z, \omega_r = \sqrt{\omega_x^2 - \omega_z^2}$  are the axial (“stretch”) and radial (“rocking”) mode frequencies for the out-of-phase motion. If the trap frequencies satisfy the condition  $\omega_s \simeq 2\omega_r$ , we can apply the standard transformations  $\hat{x} = (\hbar/4m\omega_r)^{1/2}(\hat{a} + \hat{a}^\dagger)$ ,  $\hat{u} = (\hbar/4m\omega_s)^{1/2}(\hat{c} + \hat{c}^\dagger)$  and express the Hamiltonian in the rotating wave approximation as

$$\hat{H} = \hbar\omega_r \hat{a}^\dagger \hat{a} + \hbar\omega_s \hat{c}^\dagger \hat{c} + \hbar\xi(\hat{a}^{\dagger 2} \hat{c} + \hat{a}^2 \hat{c}^\dagger), \quad (2)$$

where  $\hat{c}^\dagger, \hat{c}$  ( $\hat{a}^\dagger, \hat{a}$ ) are the phonon creation and annihilation operators in axial (radial) mode. The first two terms in Eq. (2) describe harmonic motion in the axial (radial) mode with the frequency  $\omega_s$  ( $\omega_r$ ), and the third term couples these modes with the coupling coefficient given by

$$\xi = \frac{1}{8z_0} \sqrt{\frac{\hbar\omega_s^3}{m\omega_r^2}}. \quad (3)$$

The coupling is nonlinear: one axial phonon is converted into a pair of radial phonons and vice versa.

A schematic of the experimental setup is shown in Fig. 1. Two  $^{171}\text{Yb}^+$  ions are confined in a four-rod linear rf-Paul trap [20] with the single-ion secular frequencies  $(\omega_x, \omega_y, \omega_z)/2\pi = (0.99, 0.90, 0.75)$  MHz. One of the ions is optically pumped into a metastable  $^2F_{7/2}$  state by driving the  $^2P_{1/2} \rightarrow (7/2, 2)_{3/2}$  transition (386.8 nm) with a femto-second mode-locked pulsed laser and does not interact with the laser beams during the experiment. The axial trapping frequency is controlled by dc voltages applied to the end caps, and the radial trapping potential is generated by a 30 MHz rf signal connected to diametrically opposite rods in the  $x$  direction [Fig. 1(b)]. The radial trapping frequency is actively stabilized using a pickup coil that is positioned outside the vacuum chamber at a distance of around 5 cm from the trap. The systematic drift of the radial trapping frequency  $\omega_x/2\pi$  is less than 200 Hz/h and the drift is negligible for the axial frequency.

To change the detuning  $\delta = \omega_s - 2\omega_r$ , the axial trapping frequency remains fixed for all the experiments, while the radial frequency is tuned by adjusting the dc voltages applied to the  $x$  electrodes [see Fig. 1(b)] such that only the radial mode along  $x$  interacts with the axial mode, while the radial mode along  $y$  direction is far off resonance ( $|\delta|/2\pi > 200$  kHz). The radial mode frequency  $\omega_r$  can be slowly changed between two values with the help of two identical low-pass RC filters (LPF) that have a time

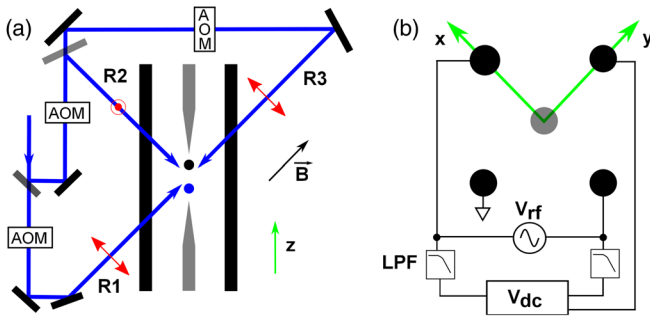


FIG. 1. (a) Schematic of the experimental setup. One of the  $\text{Yb}^+$  ions is in the  $S_{1/2}$  ground state and interacts with Doppler cooling and Raman beams. The other ion is prepared in a dark metastable  $^2F_{7/2}$  state and is sympathetically cooled. Three Raman beams  $R1$ ,  $R2$ , and  $R3$  control the motional states along the axial and radial directions. The red labels show the Raman beam polarizations. The 7.0 G magnetic field  $\vec{B}$  is parallel to the  $R1$  Raman beam. (b) Trap electrode configuration. The radial trapping potential is generated by 30 MHz rf signal  $V_{\text{rf}}$  and can be fine tuned by adjusting offset voltages on the  $x$  electrodes with two identical low-pass filters (LPF). Small additional dc voltage applied to the  $y$  electrodes helps to compensate stray electric fields.

constant of  $2 \text{ ms} \gg 2\pi/\xi$  to satisfy the adiabaticity criterion, or rapidly changed with a time constant of  $20 \mu\text{s} \ll 2\pi/\xi$  using different pairs of filters. Both time scales are much larger than one oscillation period of the ion crystal, and we have experimentally verified that no significant motional excitations are induced during these frequency sweeps [21,22].

All experimental sequences start with the detuning  $\delta/2\pi = 35$  kHz, which is much larger than  $\xi/2\pi$ , effectively decoupling two modes. Then, all the motional modes of the two-ion crystal are initialized in the ground state by Doppler cooling followed by sideband cooling [23]. For the sideband cooling of both radial and axial modes of motion, the  $R1$ - $R2$  ( $R2$ - $R3$ ) pair of Raman beams couples the axial (radial) motional mode to the internal state of the ion by driving frequency-comb-assisted Raman transitions [20,23,24], as shown in Fig. 1(a). The Raman beams are produced by a frequency-doubled mode-locked Ti:sapphire laser (pulse duration 3 ps, repetition rate 76 MHz, central wavelength 374 nm, and average power 250 mW). By adjusting the Raman detuning, we may drive the “carrier” ( $|g\rangle|n\rangle \rightarrow |e\rangle|n\rangle$ ), the “red” ( $|g\rangle|n\rangle \rightarrow |e\rangle|n-1\rangle$ ), or “blue” ( $|g\rangle|n\rangle \rightarrow |e\rangle|n+1\rangle$ ) sideband transitions. Here, the first ket state corresponds to ion internal state, namely  $|g\rangle \equiv |S_{1/2}, F=0, m_F=0\rangle$  and  $|e\rangle \equiv |S_{1/2}, F=1, m_F=0\rangle$ , and the second to the state of its motional mode. The residual population  $\bar{n}$  of all the motional modes after sideband cooling is well below 0.05 phonons.

Moreover, when the  $R1$  and  $R2$  ( $R2$  and  $R3$ ) beams are detuned from each other, the oscillating polarization gradient of the resulting optical lattice provides a periodic optical dipole force applied to the ion in the state  $|a\rangle \equiv |S_{1/2}, F=1, m_F=1\rangle$ . The ion in state  $|g\rangle$  does not experience the force because its Stark shift is independent of polarization [20].

To verify the nonlinearity of the coupling at the single-phonon level, we initially populate the radial mode with either one or two phonons. We then change dc voltages applied to the rods of the trap, with time constants of around  $20 \mu\text{s}$ , to bring the detuning  $\delta$  to zero. After time  $\tau$ , we bring the detuning back to its initial value and check for the presence of phonons in the axial or radial mode. The results are presented in Fig. 2.

We observe energy oscillations between the modes only when the radial mode is initially prepared in the two-phonon Fock state. The measured oscillation frequency  $3.02 \pm 0.02$  kHz is compatible with  $2\sqrt{2}\xi/2\pi = 2.96$  kHz predicted by Eq. (3). The reduced visibility of the oscillation and the small deviation of the measured coupling strength from theory can be attributed to two sources: the nonperfect mapping of the motional state to the internal state of the ion, and the deviation from the resonance condition, compatible with the observed frequency drifts.

The observed mode coupling is analogous to the up- and down-conversion of photons in nonlinear crystals.

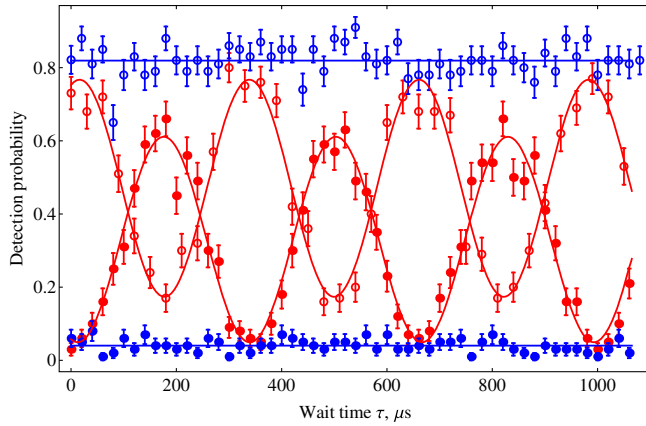


FIG. 2. Phonon state evolution in the axial (solid dots) and radial (open circles) modes, where either one (blue) or two (red) phonons are initially added to the radial mode. The sinusoidal fit (red line) reveals the coupling rate to be  $3.02 \pm 0.02$  kHz. The error bars show  $1\sigma$  statistical uncertainty. The oscillation’s amplitude after about 10 ms is a factor of  $0.39(7)$  compared to the initial amplitude, limited by the coherence time of the phonons in the radial mode [25].

However, in contrast to the optical case, where the number of pump photons required to produce one photon pair is usually large [3], the coupling strength here is much higher and this effect can be readily observed even at the single quantum level.

In order to further quantify this coupling, we probe the avoided crossing of the coupled modes of motion. Without the coupling ( $\xi \rightarrow 0$ ), the bare energy eigenstates of the Hamiltonian in Eq. (2) are degenerate and cross when  $\omega_s = 2\omega_r$ . The coupling mixes bare energy eigenstates of the system such that the new eigenstates have nonzero projection along both the axial and radial directions. This results in the mode splitting that we measure in the vicinity of the blue sideband of the axial mode as shown in Fig. 3.

If the detuning  $\delta$  changes on a time scale much longer than the inverse coupling rate  $2\pi/\xi$ , the system remains in the same energy eigenstate, leading to the adiabatic evolution of motional states between the radial and axial modes. In particular, the lowest energy eigenstate for  $\omega_s > 2\omega_r$ , i.e.,  $|n\rangle_r|0\rangle_a$ , will evolve into the lowest energy eigenstate for  $\omega_s < 2\omega_r$ . The latter eigenstate is  $|0\rangle_r|n/2\rangle_a$  for even  $n$  and  $|1\rangle_r|(n-1)/2\rangle_a$  for odd  $n$ . Therefore, the adiabatic sweep enables direct parity measurement of the ion motional state: the absence or presence of a phonon in the radial mode after the sweep determines the parity of the initial state of this mode. We detect the phonon by mapping it onto the ion internal state and then determine the expectation value of the parity operator  $\hat{P}|n\rangle_r = (-1)^n|n\rangle_r$  as  $\langle \hat{P} \rangle = (1 - 2p_1/\eta)$ , where  $\eta$  is the phonon mapping efficiency, and  $p_1$  is the probability to find the ion in the “bright” internal state after mapping.

The direct parity measurement allows the reconstruction of a quantum state’s Wigner function [26]. It was shown in

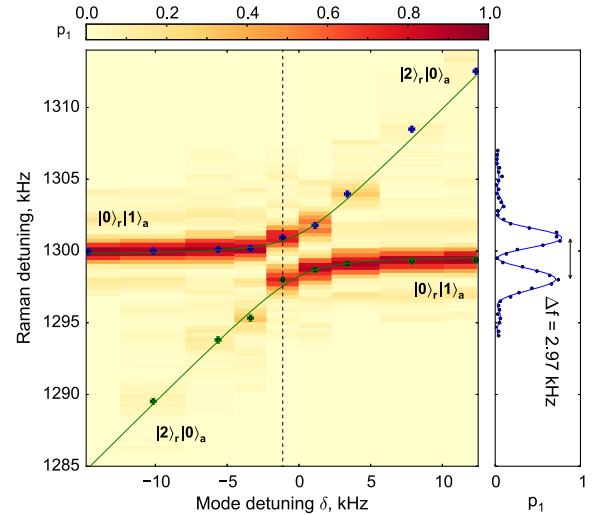


FIG. 3. Avoided crossing observed for the axial mode after sideband cooling. The left plot shows the probability  $p_1$  of the transition from a “dark”  $|F=0, m_F=0\rangle$  to “bright”  $|F=1, m_F=0\rangle$  state as a function of detuning  $\delta$  from the resonance condition, and Raman detuning. We extract the coupling strength from the mode splitting at resonance, as shown on the right panel. The splitting is measured to be  $2.97 \pm 0.03$  kHz. Dots correspond to the measured frequencies at the peak centers and the solid lines show the eigenvalues of the Hamiltonian [Eq. (2)].

[27–29] that the Wigner function relates to the parity operator by [30–33]

$$W(\alpha) = \frac{2}{\pi} \text{Tr}[D(-\alpha)\rho D(\alpha)\hat{P}],$$

where  $\rho$  is the density matrix and  $D(\alpha)$  is the displacement operator. The state  $D(-\alpha)\rho D(\alpha)$  corresponds to a displacement of the state  $\rho$  by the amount  $-\alpha$  in phase space. The displacement is done by applying a periodic force with controlled phase and duration on resonance with the radial mode of motion as described above [34]. After an adiabatic sweep of the radial trapping frequency with a time constant of 2 ms [see Fig. 1(b)], and mapping the radial phonon onto the internal state of the ion, the value of the Wigner function can be determined as  $W(\alpha) = 2\langle \hat{P} \rangle/\pi$ .

The mapping of the phonon to the internal state of the ion is achieved by applying a  $\pi$  pulse on the red sideband that simultaneously removes one phonon from the motional mode and changes the internal state of the ion. This procedure is not perfect, and is limited by the residual population of the other motional modes, power stability of the Raman lasers, and the internal state detection efficiency. To satisfy the condition  $W(\alpha) \rightarrow 0$  for large  $\alpha$ , we determine the phonon mapping efficiency to be  $\eta = 0.86 \pm 0.01$ . This value agrees well with the result of an alternative method, where the radial mode is initialized as a single-phonon Fock state and the probability of making a spin flip is subsequently found to be  $\eta = 0.89 \pm 0.04$ .

The measurement protocol of the Wigner function was tested on several quantum states, as described below. To prepare the coherent states shown in Figs. 4(b) and 4(c), we start with all the motional modes of the ion crystal cooled to the ground state [Fig. 4(a)] and apply the oscillating dipole force to coherently excite the ion motion [20,34].

To prepare the Schrödinger cat states [35] shown in Figs. 4(d)–4(f), we initialize the  $S_{1/2}$  ion in the state  $(|g\rangle + |a\rangle)|0\rangle_r/\sqrt{2}$  by the microwave  $\pi/2$  pulse and then apply an optical dipole force on resonance with the radial mode of motion. This force is spin dependent and only displaces the ion in the internal state  $|a\rangle$  [20]. After that, we swap the internal states of the ions with a microwave  $\pi$  pulse and apply the force with the phase shift  $\phi$  to produce the  $(|g\rangle|\alpha\rangle_r + |a\rangle|\alpha e^{i\phi}\rangle_r)/\sqrt{2}$  state. Finally, we apply a microwave  $\pm\pi/2$  pulse to the internal state of the ion and arrive at the state  $|g\rangle(|\alpha\rangle_r \pm |\alpha e^{i\phi}\rangle_r)/2 + |a\rangle(|\alpha\rangle_r \mp |\alpha e^{i\phi}\rangle_r)/2$ . We then detect the internal state of the ion using the standard fluorescence technique [36]. If the ion is found in the  $|g\rangle$  internal state, the ion has scattered no photons and the motional state of the ions is projected onto the Schrödinger cat state  $(|\alpha\rangle_r \pm |\alpha e^{i\phi}\rangle_r)/\sqrt{2}$ . If the ion is found in the bright state  $|a\rangle$ , the motional state is destroyed by the photon recoil and we omit these cases.

The Fock states with phonon number  $n = 1, 2$ , and 5 shown in Figs. 4(g)–4(i) are generated by the following sequence: a  $\pi$  pulse on the blue sideband of the  $|g\rangle \rightarrow |e\rangle$

transition that adds a phonon to the motional mode, followed, if necessary, by another  $\pi$  pulse on the red sideband that adds another phonon, or a  $\pi$  pulse on the carrier transition that returns the ion to the initial internal state. To generate the  $n$ -phonon Fock state  $|n\rangle_r$ ,  $n$  sideband pulses are applied.

The discrepancy between the theory and experiment in Fig. 4 is mainly due to anharmonicity of the radial motional mode, which is induced by off-resonant coupling to the vacuum state in the axial mode and causes an amplitude-dependent rotation of the Wigner function about the origin. Changes of the Wigner function due to other sources of the experimental imperfections such as motional heating ( $\leq 0.03$ ), dephasing of the motional state (up to 0.1 for the coherent and cat states), and intensity fluctuation of the Raman beams ( $\leq 0.01$ ) are smaller.

The nonlinear coupling between two modes demonstrated in this Letter, and similar coupling between three modes of the form  $\sim ab^\dagger c^\dagger + a^\dagger bc$  that requires at least three ion crystals [14], can be harnessed as a tool to study quantum effects in thermodynamics [6,7], to simulate a molecular Bose-Einstein condensate formation [9], to mimic quantum information aspects of Hawking radiation [8], implement hybrid quantum computations that involve both discrete [3] and continuous variables [4,5], and may provide sufficient nonlinearity for universal quantum computations with continuous variables [5].

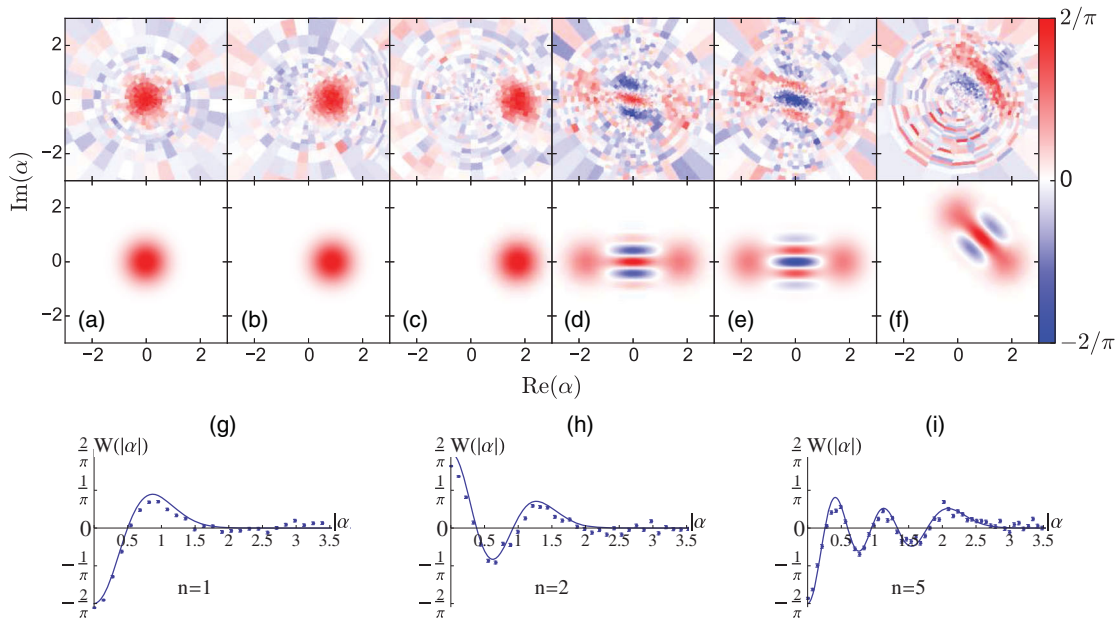


FIG. 4. Wigner functions for different quantum states. (a)–(f) Wigner functions (from left to right) for the vacuum state, coherent states  $|\alpha\rangle_r$  for  $\alpha = 0.87(3)$  and  $1.73(6)$ , Schrödinger cat states  $(|\alpha\rangle_r + |-\alpha\rangle_r)/\sqrt{2}$ ,  $(|\alpha\rangle_r - |-\alpha\rangle_r)/\sqrt{2}$ , and  $(|\alpha\rangle_r - |i\alpha\rangle_r)/\sqrt{2}$  for  $\alpha = 1.73(6)$ . The top row corresponds to the experimental data, while the bottom row shows the calculated Wigner functions. (g)–(i) Wigner functions of the Fock states  $|n\rangle_r$ , averaged over the phase of  $\alpha$  with  $n = 1, 2$ , and 5. The solid lines show the theoretical prediction  $W(|\alpha\rangle) = 2(-1)^n e^{-2|\alpha|^2} L_n(4|\alpha|^2)/\pi$ ; the points are experimentally measured values. The negative measured values of the Wigner functions for the Schrödinger cat and Fock states demonstrate the nonclassical character of these states. Reconstruction of each Wigner function requires up to 60 000 measurements and takes up to 3 h.

We acknowledge discussions with Berthold-Georg Englert, Manas Mukherjee, and Alex Kuzmich. This research was supported by the National Research Foundation and the Ministry of Education of Singapore.

*Note added.*—Recently, we became aware of parallel work of Kienzler *et al.* [37], where a different method of the Wigner function reconstruction based on the measurements in a squeezed Fock basis was demonstrated.

- 
- [1] F. Melde, *Ann. Phys. Chem.* **109**, 193 (1860).
- [2] L. Mandel and E. Wolf, *Optical Coherence and Quantum Optics* (Cambridge University Press, Cambridge, U.K., 1995).
- [3] N. K. Langford, S. Ramelow, R. Prevedel, W. J. Munro, G. J. Milburn, and A. Zeilinger, *Nature (London)* **478**, 360 (2011).
- [4] U. L. Andersen, J. S. Neergaard-Nielsen, P. van Loock, and A. Furusawa, *Nat. Phys.* **11**, 713 (2015).
- [5] S. L. Braunstein and P. van Loock, *Rev. Mod. Phys.* **77**, 513 (2005).
- [6] L. A. Correa, J. P. Palao, D. Alonso, and G. Adesso, *Sci. Rep.* **4**, 3949 (2014).
- [7] O. Abah, J. Roßnagel, G. Jacob, S. Deffner, F. Schmidt-Kaler, K. Singer, and E. Lutz, *Phys. Rev. Lett.* **109**, 203006 (2012).
- [8] P. D. Nation and M. P. Blencowe, *New J. Phys.* **12**, 095013 (2010).
- [9] G.-R. Jin, C. K. Kim, and K. Nahm, *Phys. Rev. A* **72**, 045602 (2005).
- [10] F. Lecocq, I. M. Pop, I. Matei, E. Dumur, A. K. Feofanov, C. Naud, W. Guichard, and O. Buisson, *Phys. Rev. Lett.* **108**, 107001 (2012).
- [11] E. T. Holland, B. Vlastakis, R. W. Heeres, M. J. Reagor, U. Vool, Z. Leghtas, L. Frunzio, G. Kirchmair, M. H. Devoret, M. Mirrahimi, and R. J. Schoelkopf, *Phys. Rev. Lett.* **115**, 180501 (2015).
- [12] A. Feizpour, M. Hallaji, G. Dmochowski, and A. M. Steinberg, *Nat. Phys.* **11**, 905 (2015).
- [13] D. J. Wineland, *Rev. Mod. Phys.* **85**, 1103 (2013).
- [14] C. Marquet, F. Schmidt-Kaler, and D. James, *Appl. Phys. B* **76**, 199 (2003).
- [15] X. Nie, C. F. Roos, and D. James, *Phys. Lett. A* **373**, 422 (2009).
- [16] K. R. Brown, C. Ospelkaus, Y. Colombe, A. C. Wilson, D. Leibfried, and D. J. Wineland, *Nature (London)* **471**, 196 (2011).
- [17] M. Harlander, R. Lechner, M. Brownnutt, R. Blatt, and W. Hansel, *Nature (London)* **471**, 200 (2011).
- [18] C. F. Roos, T. Monz, K. Kim, M. Riebe, H. Häffner, D. F. V. James, and R. Blatt, *Phys. Rev. A* **77**, 040302 (2008).
- [19] D. Leibfried, B. DeMarco, V. Meyer, M. Rowe, A. Ben-Kish, J. Britton, W. M. Itano, and B. Jelenković, C. Langer, T. Rosenband, and D. J. Wineland, *Phys. Rev. Lett.* **89**, 247901 (2002).
- [20] S. Ding, H. Loh, R. Hablutzel, M. Gao, G. Maslennikov, and D. Matsukevich, *Phys. Rev. Lett.* **113**, 073002 (2014).
- [21] G. Poulsen and M. Drewsen, *arXiv:1210.4309*.
- [22] A. Noguchi, Y. Shikano, K. Toyoda, and S. Urabe, *Nat. Commun.* **5**, 3868 (2014).
- [23] C. Monroe, D. M. Meekhof, B. E. King, S. R. Jefferts, W. M. Itano, D. J. Wineland, and P. Gould, *Phys. Rev. Lett.* **75**, 4011 (1995).
- [24] D. Hayes, D. N. Matsukevich, P. Maunz, D. Hucul, Q. Quraishi, S. Olmschenk, W. Campbell, J. Mizrahi, C. Senko, and C. Monroe, *Phys. Rev. Lett.* **104**, 140501 (2010).
- [25] In a Ramsey-type experiment, the coherence time of the phonons in the axial and radial modes was measured to be 55(7) ms and 10.2(9) ms, respectively. The latter is limited by trapping frequency instability and can be extended to 38(4) ms in spin-echo type measurements.
- [26] E. Wigner, *Phys. Rev.* **40**, 749 (1932).
- [27] A. Royer, *Phys. Rev. A* **15**, 449 (1977).
- [28] B.-G. Englert, N. Sterpi, and H. Walther, *Opt. Commun.* **100**, 526 (1993).
- [29] L. G. Lutterbach and L. Davidovich, *Phys. Rev. Lett.* **78**, 2547 (1997).
- [30] P. Bertet, A. Auffeves, P. Maioli, S. Osnaghi, T. Meunier, M. Brune, J. M. Raimond, and S. Haroche, *Phys. Rev. Lett.* **89**, 200402 (2002).
- [31] S. Deleglise, I. Dotsenko, C. Sayrin, J. Bernu, M. Brune, J.-M. Raimond, and S. Haroche, *Nature (London)* **455**, 510 (2008).
- [32] L. Sun, A. Petrenko, Z. Leghtas, B. Vlastakis, G. Kirchmair, K. M. Sliwa, A. Narla, M. Hatridge, S. Shankar, J. Blumoff, L. Frunzio, M. Mirrahimi, M. H. Devoret, and R. J. Schoelkopf, *Nature (London)* **511**, 444 (2014).
- [33] D. Leibfried, D. M. Meekhof, B. E. King, C. Monroe, W. M. Itano, and D. J. Wineland, *Phys. Rev. Lett.* **77**, 4281 (1996).
- [34] The amplitude of displacement  $|\alpha|$  is calibrated by measuring the average number of phonons  $\bar{n}$  in the radial mode as a function of the coherent excitation duration. The measurement yields  $|\alpha|^2 = \bar{n} = 3.0(2) \times 10^{-4} t^2$ , where  $t$  is expressed in microseconds.
- [35] C. Monroe, D. M. Meekhof, B. E. King, and D. J. Wineland, *Science* **272**, 1131 (1996).
- [36] S. Olmschenk, K. C. Younge, D. L. Moehring, D. N. Matsukevich, P. Maunz, and C. Monroe, *Phys. Rev. A* **76**, 052314 (2007).
- [37] D. Kienzler, C. Flühmann, V. Negnevitsky, H.-Y. Lo, M. Marinelli, D. Nadlinger, and J. P. Home, *Phys. Rev. Lett.* **116**, 140402 (2016).